1 **Title: Microbial oxidation of lithospheric organic carbon in rapidly eroding**
2   **tropical mountain soils**

3 **Authors:** Jordon D. Hemingway[1,2,*,†], Robert G. Hilton[3], Niels Hovius[4,5], Timothy I. Eglinton[6],
4   Negar Haghipour[6], Lukas Wacker[7], Meng-Chiang Chen[8], Valier V. Galy[1]

5 **Affiliations:**

6 [1]Woods Hole Oceanographic Institution, Department of Marine Chemistry and Geochemistry,
7 266 Woods Hole Road, Woods Hole MA 02543, USA.

8 [2]Massachusetts Institute of Technology – Woods Hole Oceanographic Institution Joint Program
9 in Oceanography and Applied Ocean Science and Engineering, 77 Massachusetts Avenue, Cam-
10 bridge MA 02139, USA.

11 [3]Durham University, Department of Geography, South Road, Durham DH1 3LE, UK.

12 [4]GFZ German Research Center for Geoscience, Telegrafenberg, Potsdam 14473, Germany.

13 [5]Department of Earth and Environmental Sciences, University of Potsdam, Karl-
14 Liebknechtstraße 24, Golm 14476, Germany.

15 [6]ETH Zürich, Geological Institute, Department of Earth Sciences, Sonneggstrasse 5, Zürich
16 8092, Switzerland.

17 [7]ETH Zürich, Laboratory of Ion Beam Physics, Department of Physics, Otto-Stern-Weg 5,
18 Zürich 8092, Switzerland.

19 [8]Taroko National Park Headquarters, Fu-Su Village, Hualien 972, Taiwan.

20 [*]Correspondence to: jordon_hemingway@fas.harvard.edu.

21 [†]Current address: Harvard University, Department of Earth and Planetary Sciences, 20 Oxford
22 Street, Cambridge MA 02138, USA.

23 **Abstract**: Lithospheric organic carbon ("petrogenic"; OC_{petro}) is oxidized during exhumation and
24 subsequent erosion within mountain ranges. This process is a significant source of CO_2 to the
25 atmosphere over geologic timescales, but the mechanisms that govern oxidation rates in
26 mountain landscapes remain poorly constrained. We demonstrate that, on average, 67 ± 11 % of
27 OC_{petro} initially present in bedrock exhumed from the tropical, rapidly eroding Central Range of
28 Taiwan is oxidized within soils, leading to CO_2 emissions of $6.1 - 18.6$ t C km^{-2} yr^{-1}. The
29 molecular and isotopic evolution of bulk OC and lipid biomarkers during soil formation reveals
30 that OC_{petro} remineralization is microbially mediated. Rapid oxidation in mountain soils drives
31 CO_2 emissions fluxes that increase with erosion rate, thereby counteracting CO_2 drawdown by
32 silicate weathering and biospheric OC burial.

33 **One Sentence Summary:** Oxidation of lithospheric organic carbon in eroding mountain soils is
34 rapid and microbially mediated, and resulting CO_2 emissions counteract CO_2 drawdown by
35 silicate weathering and biospheric organic carbon burial.

Main Text: Erosion-induced weathering in collisional mountain belts is a major carbon-cycle regulator over million-year timescales and provides a link between tectonics and climate (*1*, *2*). Atmospheric CO_2 is consumed by the export and burial in marine sediments of biospheric organic carbon (OC_{bio}) and carbonate minerals precipitated following silicate rock weathering (*1*). The CO_2 drawdown flux associated with both processes increases with erosion rate (*3*, *4*), highlighting the importance of steep, erosive orogens in driving CO_2 drawdown. By comparison, CO_2 release during exhumation and erosion has received considerably less attention despite its potential to partially or fully negate the effects of geological CO_2 consumption (*1*, *5*, *6*). Oxidative weathering of both sulfide minerals (coupled with carbonate dissolution) and petrogenic organic carbon (OC_{petro}) contained in exhumed rocks can increase atmospheric CO_2 and decrease O_2 concentrations over geologic timescales (*1*, *7-9*). Still, the mechanisms that govern oxidation rates and efficiencies in mountain belts remain under-constrained (*5*, *8*, *9*).

To better constrain orogenic CO_2 emissions, we assess the controls on OC_{petro} oxidation and export within the Central Range of Taiwan, one of the fastest exhuming and eroding mountain belts on Earth (*10*). Steep relief (*11*), frequent typhoon landfall (*10*), and high bedrock landslide rates (*11*) lead to long-term erosion rates of $3 - 6$ mm yr^{-1} across the range (*10*). While supplemental contributions from deeper in the exhumation path are likely, weathering in such mountain landscapes occurs primarily on hillslopes and in colluvial deposits (*12*, *13*). We therefore assess OC molecular and isotopic evolution within multiple hillslope soil profiles located in the LiWu and WuLu River basins (**Fig. S1**) and verify these observations at the catchment scale using LiWu River suspended sediments (*14*). Soils at our study sites are ≤ 1 m thick, including mineral (A+E) and saprolite (C) layers (*15*), experience residence times on the order of centuries (*14*), and overlay bedrock ranging from Mesozoic greenschist and amphibolite at low elevations (Tananao schists) to Cenozoic slate and phyllite near the Lishan Fault (Pilushan and Lushan formations) (*16*). All lithologies are carbonaceous, with bedrock outcrops containing $0.2 - 0.7$ % OC_{petro} (**Table S1**) (*17*).

Significant OC_{petro} loss is observed in all soil profiles, as evidenced by the relationship between soil OC content (% OC_{soil}) and ^{14}C activity (expressed as "fraction modern" or Fm) (*14*). To account for differences in % OC between bedrock lithologies (*17*), % OC_{soil} is expressed as

$$\Delta\%OC = \% \ OC_{soil} - \% \ OC_{bedrock}, \tag{1}$$

where % $OC_{bedrock}$ is the OC content of bedrock immediately underlying each soil sample. The average fraction of bedrock OC that is oxidized during soil formation, f_{ox}, can then be quantified by utilizing the fact that OC_{petro} is inherently ^{14}C-free ($Fm_{petro} = 0.0$) and setting $Fm_{bio} = 1.045 \pm 0.079$, the measured ^{14}C activity of vascular plant leaf-wax fatty acids extracted form A+E horizon soils (**Table S2**) (*14*). Soil OC is treated as a mixture of OC_{bio} and residual OC_{petro}, leading to the equation (*14*):

$$Fm_{soil} = Fm_{bio} \left[\frac{\Delta\%OC + (f_{ox})(\% \ OC_{bedrock})}{\Delta\%OC + \% \ OC_{bedrock}} \right]. \tag{2}$$

Fm_{soil} is a hyperbolic function of $\Delta\%OC$ with curvature that is defined by both %$OC_{bedrock}$ and f_{ox}, as shown in **Fig 1**. We simultaneously solve **Eq. 2** for the best-fit % $OC_{bedrock}$ and f_{ox} values using orthogonal distance regression and account for uncertainty using Monte Carlo resampling (*14*).

On average, 67 ± 11 % ($\pm 1\sigma$) of bedrock OC is lost during soil formation, a minimum estimate since deep weathering has likely already removed OC from initial bedrock (*18*). To test if observed % OC trends simply reflect mobile element losses during weathering and not oxidation *per se*, we solve **Eq. 2** for a subset of samples after normalizing OC content to the immobile element titanium (**Table S1**) (*14*). Calculated f_{ox} values using normalized and un-normalized data are identical within uncertainty, indicating no appreciable mobility effect on our results (**Fig. S2**).

Assuming that all OC lost is oxidized to CO_2 (*8*), f_{ox} can be used to estimate the steady-state CO_2 emission flux from soils due to OC_{petro} oxidation, termed Φ_{ox}, according to

$$\Phi_{ox} = \frac{(f_{ox})(\% \; OC_{bedrock})(\rho_{soil})(z_{soil})}{\tau_{soil}}, \tag{3}$$

where ρ_{soil} is the soil density, z_{soil} is the soil thickness (*15*), and τ_{soil} is the soil residence time on hillslopes. We estimate τ_{soil} using three independent methods (landslide rates, catchment-average denudation rates, OC_{bio} erosion rates) and incorporate uncertainty for each variable in **Eq. 3** using Monte Carlo resampling across the range of observed values (*14*), resulting in a median Φ_{ox} range of $6.1 - 18.6$ t C km^{-2} yr^{-1} for conditions prevalent across the Central Range (**Fig. S3A**) (*14*). We emphasize that Φ_{ox} is a minimum estimate of total CO_2 emissions by OC_{petro} oxidation due to the potential for OC losses occurring during deep weathering (*18*). Still, this flux is statistically identical to two independent, catchment-integrated OC_{petro} oxidation estimates for Taiwanese rivers based on fluvial OC_{petro} export (≤ 12 t C km^{-2} yr^{-1}) (*19*) and dissolved rhenium yield ($7 - 13$ t C km^{-2} yr^{-1}; **Fig. S3B**) (*5*) and is 2- to 6-fold higher than estimates of CO_2 drawdown by silicate weathering in the LiWu catchment (**Fig. S3C**) (*18*). The observation that Φ_{ox} matches catchment-integrated emissions implies that OC_{petro} oxidation in Taiwan occurs predominantly within rapidly eroding hillslope soils.

A saprolite depth profile collected from the WuLu catchment indicates that bedrock OC can be oxidized and replaced with OC_{bio} before A+E horizons have fully developed. Two samples collected at 0.5 m and 0.2 m depth contain similar OC concentrations (0.20 %, 0.28 %, respectively) but drastically different Fm values (0.108, 0.839, respectively; **Table S1**). Rapid OC_{petro} oxidation can occur (i) abiotically without chemical alteration, (ii) abiotically with chemical alteration, (iii) biotically without chemical alteration, or (iv) biotically with chemical alteration and ^{14}C-depleted biomass production (*20-22*). To assess alteration and to track multiple OC sources within a single sample, we utilize Ramped PyrOx (RPO) serial combustion (*23*). This technique heats each sample at a constant ramp rate to separate OC based on thermal lability and determines Fm values for specific temperature intervals (termed RPO fractions) (*14*). To quantitatively compare OC chemical structure, we determine the underlying thermal activation energy (E) distribution for each sample, termed $p(0,E)$, as this is an intrinsic property of carbon bond strength and thus a proxy for chemical composition (*23*). Unlike ^{14}C activity, end-member mixing does not shift OC in E space. Mixing OC_{bio} with unaltered OC_{petro} will thus result in a bimodal $p(0,E)$ distribution, whereas chemical alteration is required to explain the presence of intermediate E values (*14, 23*).

We constrain bedrock E using particulate OC (POC) from 27 suspended sediment samples, including isolated ≥ 2 mm clasts, collected from the LiWu River during four typhoon events (*14*). Because sediment exported during typhoons is dominated by material sourced from

120 bedrock incision, distributed runoff erosion, and landsliding throughout the basin (*11*, *12*), we
121 expect this sample set to integrate outcropped bedrock lithologies that contain relatively
122 unweathered OC_{petro}. This is supported by bulk POC ^{13}C content (expressed as $\delta^{13}C$ values) and
123 total nitrogen to POC ratios (**Table S3**), which span the range of Tananao schist, Lushan
124 formation, and Pilushan formation values (*17*). **Fig. 2A** shows that bedrock OC is exclusively
125 associated with $E \geq 185$ kJ mol^{-1} (termed high-*E*; **Fig. S3A**) (*14*), consistent with the observed
126 partial graphitization of this material (*16*). We additionally constrain vascular-plant OC $p(0,E)$
127 using two organic-rich (≥ 5 %) surface soils characterized by bulk Fm values similar to those of
128 plant-wax fatty acids (*14*). For both samples, ≥ 90 % of OC is associated with $E < 150$ kJ mol^{-1}
129 (termed low-*E*), indicating that OC_{bio} and OC_{petro} are effectively separated in *E* space.
130   Energy distributions and ^{14}C activity in soil and saprolite materials provide strong
131 evidence for OC_{petro} chemical alteration during weathering. Up to 51 % of OC contained in
132 saprolites and deep A+E horizons lies between 150 and 185 kJ mol^{-1} (termed mid-*E*; **Table S4**;
133 **Fig. S4B-C**); higher than that corresponding to vascular-plant OC (< 150 kJ mol^{-1}) yet lower
134 than bedrock OC (≥ 185 kJ mol^{-1}). This observation can result from either (i) increasing
135 vascular-plant OC *E* by stabilization during aging in soils (*24*) or (ii) decreasing residual OC_{petro}
136 *E* during oxidative weathering (*20, 21*). We assess the relative importance of these mechanisms
137 using the ^{14}C activity of each RPO fraction (**Table S5**). As shown in **Fig. 2B**, low-*E* Fm values
138 cluster near those of vascular-plant fatty acids, whereas high-*E* material approaches Fm of zero.
139 Meanwhile, mid-*E* OC spans an Fm range from 0.083 ± 0.002 to 0.912 ± 0.008. We rule out the
140 possibility that ^{14}C-depleted mid-*E* OC exclusively reflects OC_{bio} aging because (i) this would
141 require a biospheric component that has aged up to 20,000 ^{14}C yr, significantly longer than the
142 centennial soil residence times in Taiwan (*14*), and (ii) plant-wax fatty acids are not detected in
143 some saprolite samples (**Table S6**). Thus, mid-*E* material must reflect a mixture of weathered
144 OC_{petro} and moderately aged OC_{bio}.
145   We treat OC_{petro} that has been chemically altered during weathering as a unique end
146 member described by Fm = 0.0 and a value of f_{mid}, the fraction of $p(0,E)$ contained within the
147 mid-*E* range, greater than the highest observed saprolite value of 0.51 (*14*). **Fig. 3A** shows that
148 all hillslope samples, with the exception of one unweathered saprolite, are adequately explained
149 by a mixture of OC_{bio} and chemically altered OC_{petro}. This end member is also observed in LiWu
150 River POC collected during typhoon floods, as evidenced by the divergence from a vertical
151 mixing line between OC_{petro} and OC_{bio} in **Fig. 3A**. Therefore, along with unweathered bedrock
152 OC (*19*) sourced from deep incision and landsliding (*11*), we detect catchment-scale export of
153 chemically altered OC_{petro} from Central Range hillslopes during typhoon flood events. Because
154 calculated f_{mid} depends on our choice of mid-*E* range (here, 150 to 185 kJ mol^{-1}), it is possible
155 that mixing trends and end-member compositions are sensitive to changes in *E* boundary values.
156 We test this sensitivity by allowing these boundary values to vary by ± 10 kJ mol^{-1} (*14*).
157 Although quantitative differences exist (**Fig. S5**), resulting mixing trends are qualitatively robust,
158 indicating that the importance of chemically altered OC_{petro} is insensitive to our choice of mid-*E*
159 boundary values.
160   Fatty acid molecular distributions and $\delta^{13}C$ values imply that rapidly oxidized OC_{petro} in
161 soils is incorporated into microbial biomass, supporting laboratory-based incubation studies (*20,
162 22*). We calculate $f_{microbial}$, the fraction of total fatty acids that are microbial in origin (*25, 26*), as
163 a proxy for the relative abundance of heterotrophic vs. vascular-plant biomass (*14*). This

164   approach excludes fungal contributions and is thus a minimum estimate of heterotrophic
165   biomass. **Fig. 3B** shows that bulk Fm is negatively correlated with $f_{microbial}$ across all soil and
166   POC samples. We do not expect this trend to be linear due to fatty acid production biases (*25,*
167   *26*). Still, this relationship clearly suggests that heterotrophic biomass is more abundant in
168   samples containing predominantly ^{14}C-free OC.
169   Sample limitation prevented measurement of microbial fatty acid ^{14}C activity (*14*), but
170   their $\delta^{13}C$ values imply that bedrock OC is used as substrate (**Table S7**) (*26, 27*). Bulk OC and
171   plant-wax fatty acid $\delta^{13}C$ values correlate strongly in A+E horizons ($r^2 = 0.959$; *p*-val < 0.001; *n*
172   = 7), reflecting the predominance of OC_{bio} in these samples, but are uncorrelated in C-horizons
173   (*p*-val > 0.05; *n* = 4) due to a lack of significant OC_{bio} contribution to saprolites (**Fig. S6**). Still, if
174   OC_{bio} were the sole substrate for heterotrophs, then microbial and plant-wax fatty acid $\delta^{13}C$
175   values should correlate strongly with a constant $\delta^{13}C$ offset (*27*) in all samples. This is not
176   observed in either A+E horizon (*p*-val > 0.05; *n* = 7) or saprolite (*p*-val > 0.05; *n* = 4) samples,
177   indicating that vascular plant OC cannot be the only substrate. Rather, this lack of correlation
178   requires a secondary microbial carbon source (*20-22*), namely bedrock OC. We conclude that
179   mid-*E*, ^{14}C-free material is a product of microbial bedrock oxidation, produced either directly by
180   extracellular enzymes or indirectly after acid hydrolysis (*20*), and is manifest as ^{14}C-depleted
181   living biomass (*22*) or as residual, chemically altered OC_{petro} (*21*).
182   Substantial bedrock OC replacement within saprolites implies that significant weathering
183   occurs ≤ 1 m below the surface and that microbially mediated OC_{petro} oxidation can proceed at a
184   pace matching the rapid exhumation in Taiwan. We propose that exhumation and hillslope
185   erosion rates exert a first-order control on CO_2 emissions from OC_{petro} oxidation, as faster
186   erosion will increase the rate of bedrock exposure to the weathering front (*8*). This is further
187   supported by measurements of the dissolved rhenium flux from Taiwanese rivers, a proxy for
188   OC_{petro} oxidation, which increases with erosion rate (*5*). However, the relationship between
189   OC_{petro} oxidation and physical erosion rate cannot be linear. Large earthquakes and typhoons are
190   known to cause widespread bedrock landsliding (*28-30*) and elevated export of OC_{petro} by rivers
191   (*19*). Such events increase catchment-averaged erosion rates (*28*), but could decrease catchment-
192   averaged OC_{petro} oxidation efficiency by bypassing the hillslope soil weathering window. OC_{petro}
193   remineralization in Taiwan is incomplete, as evidenced by the abundance of bedrock OC in
194   sediments exported by rivers (*19*) and deposited in nearby coastal margins (*31*). We predict a
195   dampened response of OC_{petro}-derived CO_2 emissions to further erosion rate increases, as
196   increasing landslide rates will result in less catchment area that is available for soil formation and
197   weathering.
198   Microbially mediated oxidative weathering in Taiwanese hillslope soils offsets geologic
199   CO_2 drawdown and O_2 production by silicate weathering and OC_{bio} burial (*1, 5, 8, 22*). The Φ_{ox}
200   range calculated here is similar in magnitude to CO_2 source estimates from sulfide oxidation (≥
201   22.9 ± 1.0 t C km^{-2} yr^{-1}; LiWu basin only) (*9*), as well as CO_2 sinks from silicate weathering (3.1
202   ± 0.1 t C km^{-2} yr^{-1}; LiWu basin only; **Fig. S3C**) (*18*) and OC_{bio} burial (21 ± 10 t C km^{-2} yr^{-1};
203   Taiwan average; **Fig. S3D**) (*14, 32*). This process is likely globally significant, as rapid soil
204   formation is observed in other tropical and temperate orogenic settings such as the Southern Alps
205   of New Zealand (*33*). We therefore hypothesize that CO_2 consumption is not favored within
206   highly erosive mountain belts dominated by OC- and sulfide-rich low- and intermediate-grade
207   metasedimentary lithologies. This results from the observation that OC_{petro} and sulfide mineral

208   oxidation is not limited by reaction kinetics even at high erosion rates (*5, 8, 21*), unlike silicate
209   weathering and OC_{bio} export (*4, 34*). Conversely, the magnitude of the net CO_2 sink likely
210   increases with physical erosion rate in orogens dominated by high-grade metamorphic and
211   igneous rocks due to their lower OC_{petro} and sulfide contents. While the global fluxes and the
212   timescales over which they impact atmospheric CO_2 and O_2 concentrations remain to be
213   assessed, our results demonstrate the importance of microbially mediated OC_{petro} oxidation and
214   its relationship to tectonic and erosive controls on the global carbon cycle and Earth's long-term
215   climate.

References and Notes:

1. N. M. Bergman, T. M. Lenton, A. J. Watson, COPSE: A new model of biogeochemical cycling over Phanerozoic time. *Am. J. Sci.* **304**, 397–437 (2004).

2. P. Molnar, P. England, Late Cenozoic uplift of mountain ranges and global climate change: Chicken or egg? *Nature*. **346**, 29–34 (1990).

3. J. Gaillardet, B. Dupré, P. Louvat, C. J. Allègre, Global silicate weathering and CO_2 consumption rates deduced from the chemistry of large rivers. *Chem. Geol.* **159**, 3–30 (1999).

4. V. V. Galy, B. Peucker-Ehrenbrink, T. I. Eglinton, Global carbon export from the terrestrial biosphere controlled by erosion. *Nature*. **521**, 204–207 (2015).

5. R. G. Hilton, J. Gaillardet, D. Calmels, J.-L. Birck, Geological respiration of a mountain belt revealed by the trace element rhenium. *Earth Planet. Sci. Lett.* **403**, 27–36 (2014).

6. M. A. Torres, A. J. West, K. E. Clark, G. Paris, J. Bouchez, C. Ponton, S. J. Feakins, V. Galy, J. F. Adkins, The acid and alkalinity budgets of weathering in the Andes–Amazon system: Insights into the erosional control of global biogeochemical cycles. *Earth Planet. Sci. Lett.* **450**, 381–391 (2016).

7. R. A. Berner, K. Caldeira, The need for mass balance and feedback in the geochemical carbon cycle. *Geology*. **25**, 955–956 (1997).

8. E. W. Bolton, R. A. Berner, S. T. Petsch, The weathering of sedimentary organic matter as a control on atmospheric O_2: II. Theoretical modeling. *Am. J. Sci.* **306**, 575–615 (2006).

9. M. A. Torres, A. J. West, G. Li, Sulphide oxidation and carbonate dissolution as a source of CO_2 over geological timescales. *Nature*. **507**, 346–349 (2014).

10. S. Dadson, J. Hovius, H. Chen, W. B. Dade, M.-L. Hsieh, S. D. Willett, J.-C. Hu, M.-J. Horng, M.-C. Chen, C. P. Stark, D. Lague, J.-C. Lin, Links between erosion, runoff variability and seismicity in the Taiwan orogen. *Nature*. **426**, 648–651 (2003).

11. N. Hovius, C. P. Stark, H.-T. Chu, J.-C. Lin, Supply and removal of sediment in a landslide-dominated mountain belt: Central Range, Taiwan. *J. Geol.* **108**, 73–89 (2000).

12. R. Emberson, N. Hovius, A. Galy, O. Marc, Oxidation of sulfides and rapid weathering in recent landslides. *Earth Surf. Dynam.* **4**, 727–742 (2016).

13. K. Maher, C. P. Chamberlain, Hydrologic regulation of chemical weathering and the geologic carbon cycle. *Science*. **343**, 1502–1504 (2014).

14. Materials and methods are available as supplementary materials on *Science Online*.

15. C.-C. Tsai, Z.-S. Chen, C.-T. Duh, F.-W. Horng, Prediction of soil depth using a soil–landscape regression model: A case study on forest soils in southern Taiwan. *Proc. Nat. Sci. Counc. ROC(B)*. **25**, 34–39 (2001).

16. O. Beyssac, M. Simoes, J. P. Avouac, K. A. Farley, Y.-G. Chen, Y.-C. Chan, B. Goffé, Late Cenozoic metamorphic evolution and exhumation of Taiwan. *Tectonics*. **26**, TC6001 (2007).

17. R. G. Hilton, A. Galy, N. Hovius, M.-J. Horng, H. Chen, The isotopic composition of particulate organic carbon in mountain rivers of Taiwan. *Geochim. Cosmochim. Acta*. **74**, 3164–3181 (2010).

18. D. Calmels *et al.*, Contribution of deep groundwater to the weathering budget in a rapidly eroding mountain belt, Taiwan. *Earth Planet. Sci. Lett.* **303**, 48–58 (2011).

19. R. G. Hilton, A. Galy, N. Hovius, M.-J. Horng, H. Chen, Efficient transport of fossil organic

carbon to the ocean by steep mountain rivers: An orogenic carbon sequestration mechanism. *Geology.* **39**, 71–74 (2011).

20. S. Schillawski, S. Petsch, Release of biodegradable dissolved organic matter from ancient sedimentary rocks. *Glob. Biogeochem. Cy.* **22**, GB3002 (2008).

21. S. Chang, R. A. Berner, Coal weathering and the geochemical carbon cycle. *Geochim. Cosmochim. Acta.* **63**, 3301–3310 (1999).

22. S. T. Petsch, T. I. Eglinton, K. J. Edwards, ^{14}C-dead living biomass: Evidence for microbial assimilation of ancient organic carbon during shale weathering. *Science.* **292**, 1127–1131 (2001).

23. J. D. Hemingway, D. H. Rothman, S. Z. Rosengard, V. V. Galy, Technical note: An inverse method to relate organic carbon reactivity to isotope composition from serial oxidation. *Biogeosciences* **14**, 5099–5114 (2017).

24. R. G. Keil, L. M. Mayer, "Mineral matrices and organic matter" in *Treatise on Geochemistry*, H. Holland, K. Turekian, Eds. (Elsevier, 2014), vol. 12, chap. 12.

25. A. Frostegård, E. Bååth, The use of phospholipid fatty acid analysis to estimate bacterial and fungal biomass in soil. *Biol. Fertil. Soils.* 22, 59–65 (1996).

26. F. M. Hopkins, T. R. Filley, G. Gleixner, M. Lange, S. M. Top, S. E. Trumbore, Increased belowground carbon inputs and warming promote loss of soil organic carbon through complementary microbial responses. *Soil Biol. Biochem.* **76**, 57–69 (2014).

27. N. E. Blair, A. Leu, E. Muñoz, J. Olsen, E. Kwong, D. des Marais, Carbon isotopic fractionation in heterotrophic microbial metabolism. *Appl. Environ. Microbiol.* **50**, 996–1001 (1985).

28. N. Hovius, P. Meunier, C.-W. Lin, H. Chen, Y.-G. Chen, S. Dadson, M.-J. Horng, M. Lines, Prolonged seismically induced erosion and the mass balance of a large earthquake. *Earth Planet. Sci. Lett.* **304**, 347–355 (2011).

29. G. Li, A. J. West, A. L. Densmore, Z. Jin, F. Zhang, J. Wang, M. Clark, R. G. Hilton, Earthquakes drive focused denudation along a tectonically active mountain front. *Earth Planet. Sci. Lett.* **472**, 253–265 (2017).

30. O. Marc, N. Hovius, P. Meunier, Uchida, T. & Gorum, T.: A physically-based expression for the area and volume of earthquake-triggered landslide populations. *JGR-ES,* **121**, 640-663 (2016).

31. L.-W. Zheng, X. Ding, J. T. Liu, D. Li, T.-Y. Lee, X. Zheng, Z. Zheng, M. N. Xu, M. Dai, S.-J. Kao, Isotopic evidence for the influence of typhoons and submarine canyons on the sourcing and transport behavior of biospheric organic carbon to the deep sea. *Earth Planet. Sci. Lett.* **465**, 103–111 (2017).

32. R. G. Hilton, A. Galy, N. Hovius, S.-J. Kao, M.-J. Horng, H. Chen, Climatic and geomorphic controls on the erosion of terrestrial biomass from subtropical mountain forest. *Global Biogeochem. Cy.* **26**, GB3014 (2012).

33. I. J. Larsen, P. C. Almond, A. Eger, J. O. Stone, D. R. Montgomery, B. Malcolm, Rapid soil production and weathering in the Southern Alps, New Zealand. *Science.* **343**, 637–640 (2014).

34. A. J. West, Thickness of the chemical weathering zone and implications for erosional and climatic drivers of weathering and for carbon-cycle feedbacks. *Geology.* **40**, 811–814 (2012).

304 35. R. G. Hilton, A. J. West, A. Galy, N. Hovius, G. G. Roberts, Geomorphic control on the δ^{15}N
305   of mountain forests. *Biogeosciences*. **10**, 1693–1705 (2013).
306 36. R. G. Hilton, A. Galy, N. Hovius, M.-C. Chen, M.-J. Horng, H. Chen, Tropical-cyclone-
307   driven erosion of the terrestrial biosphere from mountains. *Nat. Geosci*. **1**, 759–762
308   (2008).
309 37. J. M. Turowski, N. Hovius, M.-L. Hsieh, D. Lague, M.-C. Chen, Distribution of erosion
310   across bedrock channels. *Earth Surf. Process. Landforms*. **33**, 353–363 (2008).
311 38. J. H. Whiteside, P. E. Olsen, T. I. Eglinton, B. Cornet, N. G. McDonald, P. Huber, Pangean
312   great lake paleoecology on the cusp of the end-Triassic extinction. *Palaeoceanogr.,*
313   *Palaeoclim., Palaeoecol.* **301**, 1–17 (2011).
314 39. J. D. Hemingway, V. V. Galy, A. R. Gagnon, K. E. Grant, S. Z. Rosengard, G. Soulet, P. K.
315   Zigah, A. P. McNichol, Assessing the blank carbon contribution, isotope mass balance,
316   and kinetic isotope fractionation of the ramped pyrolysis/oxidation instrument at
317   NOSAMS. *Radiocarbon*. **59**, 179–193 (2017).
318 40. B. E. Rosenheim, M. B. Day, E. Domack, H. Schrum, A. Benthien, J. M. Hayes, Antarctic
319   sediment chronology by programmed-temperature pyrolysis: Methodology and data
320   treatment. *Geochem. Geophys. Geosyst.* **9**, Q04005 (2008).
321 41. J. D. Hemingway, E. Schefuß, B. J. Dinga, H. Pryer, V. V. Galy, Multiple plant-wax
322   compounds record differential sources and ecosystem structure in large river catchments.
323   *Geochim. Cosmochim. Acta*. **184**, 20–40 (2016).
324 42. V. V. Galy, T. I. Eglinton, Protracted storage of biospheric carbon in the Ganges-
325   Brahmaputra basin. *Nat Geosci*. **4**, 843–847 (2011).
326 43. A. L. Sessions, Isotope-ratio detection for gas chromatography. *J. Sep. Sci.* **29**, 1946–1961
327   (2006).
328 44. P. J. Reimer, T. A. Brown, R. W. Reimer, Discussion: Reporting and calibration of post-
329   bomb ^{14}C data. *Radiocarbon*. **46**, 1299–1304 (2004).
330 45. A. P. McNichol, G. A. Jones, D. L. Hutton, A. Gagnon, R. M. Key, The Rapid Preparation of
331   Seawater ΣCO_2 for Radiocarbon Analysis at the National Ocean Sciences AMS Facility.
332   *Radiocarbon*. **36**, 237–246 (1994).
333 46. A. Pearson, A. P. McNichol, R. J. Schneider, K. F. von Reden, Y. Zheng, Microscale AMS
334   ^{14}C measurement at NOSAMS. *Radiocarbon*. **40**, 61–75 (1998).
335 47. C. P. McIntyre, L. Wacker, N. Haghipour, T. M. Blattmann, S. Fahrni, M. Usman, T. I.
336   Eglinton, H.-A. Sayno, Online ^{13}C and ^{14}C gas measurements by EA-IRMS-AMS at ETH
337   Zürich. *Radiocarbon* **59**, 893–903 (2017).
338 48. K. Fornace, "Late Quaternary climate variability and terrestrial carbon cycling in tropical
339   South America," thesis, MIT/WHOI (2016).
340 49. B. P. Boudreau, B. R. Ruddick, On a reactive continuum representation of organic matter
341   diagenesis. *Am. J. Sci.* **291**, 507–538 (1991).
342 50. T. I. Eglinton, G. Eglinton, Molecular proxies for paleoclimatology. *Earth Planet. Sci. Lett.*
343   **275**, 1–16 (2008).
344 51. P. A. Meyers, R. Ishiwatari, Lacustrine organic geochemistry – An overview of indicators of
345   organic matter sources and diagenesis in lake sediments. *Org. Geochem.* **20**, 867–900
346   (1993).
347 52. D. M. Glover, W. J. Jenkins, S. C. Doney, "Least squares and regression techinques,

348   goodness of fit and tests, and nonlinear least squares techniques," in *Modeling Methods*
349   *for Marine Science* (Cambridge University Press, New York, ed. 1, 2011), pp. 49–74.

350 53. G.-W. Lin, H. Chen, N. Hovius, M.-J. Horng, S. Dadson, P. Meunier, M. Lines, Effects of
351   earthquake and cyclone sequencing on landsliding and fluvial sediment transfer in a
352   mountain catchment. *Earth Surf. Process. Landforms*. **33**, 1354–1373 (2008).

353 54. J.-C. Chang, O. Slaymaker, Frequency and spatial distribution of landslides in a mountainous
354   drainage basin: Western Foothills, Taiwan. *Catena*. **46**, 285–307 (2002).

355 55. K.-T. Chang, S.-H. Chiang, M.-L. Hsu, Modeling typhoon- and earthquake-induced
356   landslides in a mountainous watershed using logistic regression. *Geomorphology*. **89**,
357   335–347 (2007).

358 56. Y.-C. Chen, K.-T. Chang, Y.-J. Chiu, S.-M. Lau, H.-Y. Lee, Quantifying rainfall controls on
359   catchment-scale landslide erosion in Taiwan. *Earth Surf. Process. Landforms*. **38**, 372–
360   382 (2013).

361 57. Y.-C. Chen, K.-T. Chang, H.-Y. Lee, S.-H. Chiang, Average landslide erosion rate at the
362   watershed scale in southern Taiwan estimated from magnitude and frequency of rainfall.
363   *Geomorphology*. **228**, 756–764 (2015).

364 58. Y. Tang, J. K. Perry, P. D. Jenden, M. Schoell, Mathematical modeling of stable carbon
365   isotope ratios in natural gases. *Geochim. Cosmochim. Acta*. **64**, 2637–2687 (2000).

366 59. J. D. Hemingway, *rampedpyrox*: Open-source tools for thermoanalytical data analysis, 2016-
367   , http://pypi.python.org/pypi/rampedpyrox, DOI: 10.5281/zenodo.839815 (2017).

368 60. E. K. Williams, B. E. Rosenheim, A. P. McNichol, C. A. Masiello, Charring and non-
369   additive chemical reactions during ramped pyrolysis: Applications to the characterization
370   of sedimentary and soil organic material. *Org. Geochem.* **77**, 106–114 (2014).

371 61. L. Zelles, Phospholipid fatty acid profiles in selected members of soil microbial
372   communities. *Chemosphere* **35**, 275–294 (1997).

373 62. A. Das, C.-H. Chung, C.-F. You, Disproportionately high rates of sulfide oxidation from
374   mountainous river basins of Taiwan orogeny: Sulfur isotope evidence. *Geophys. Res.*
375   *Lett*. **39**, L12404 (2012).

376 63. L. Mesalles, F. Mouthareau, M. Bernet, C.-P. Chang, A. T.-S. Lin, C. Fillon, X. Sengelen,
377   From submarine continental accretion to arc-continent orogenic evolution: The thermal
378   record in southern Taiwan. *Geology*. **42**, 907–910 (2014).

379 64. C. France-Lanord, L. A. Derry, Organic carbon burial forcing of the carbon cycle from
380   Himalayan erosion. *Nature*. **390**, 65–67 (1997).

381 65. L. S. Teng, Geotectonic evolution of late Cenozoic arc-continent collision in Taiwan.
382   *Tectonophysics*. **183**, 57–76 (1990).

391 and L.W. performed laboratory measurements; J.D.H., R.G.H., N. Haghipour, L.W., and V.V.G.
392 analyzed data; J.D.H., R.G.H., N. Hovius, and V.V.G. wrote the manuscript with input from all
393 authors.
394

395
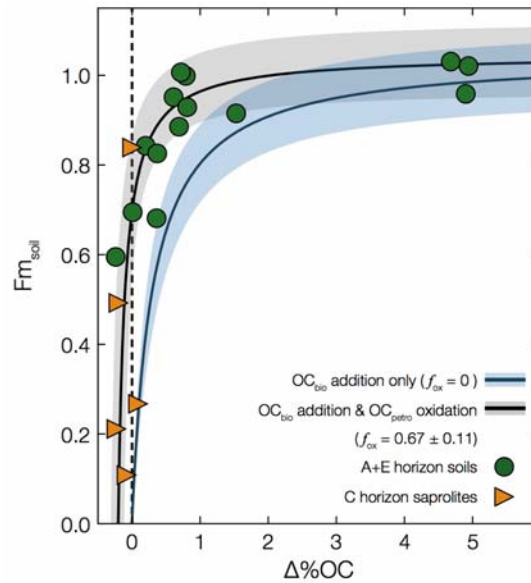
Fig. 1. Evidence for bedrock OC oxidation. Blue line is the solution to **Eq. 2** assuming no
OC_{petro} oxidation during soil formation (OC_{bio} addition only; $f_{ox} = 0$). Black line is the orthogonal
distance regression best-fit solution that minimizes the residual error between measured (green
circles, orange triangles) and predicted Fm_{soil} values. Shaded region for both trends is the
propagated $\pm 1\sigma$ uncertainty (*14*). Best-fit results indicate that 67 ± 11 % of bedrock OC is lost
during oxidative weathering. $\Delta\%OC = 0$ is shown as a vertical dashed line. Measurement error
bars are smaller than marker sizes.

403

404
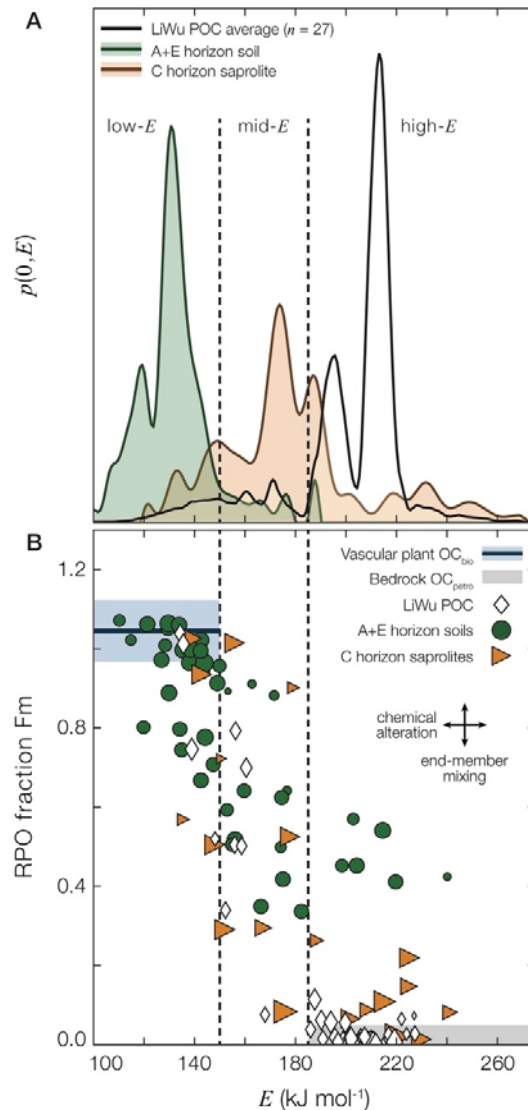
Fig. 2. Evidence for OC$_{petro}$ chemical alteration. (**A**) Representative $p(0,E)$ distributions highlighting the differences between OC end members: average of LiWu POC exported during typhoon events ($n = 27$; black), organic-rich A+E horizon topsoil (green), and C horizon saprolite (orange). Each $p(0,E)$ distribution integrates to unity (y-axis values not shown) (*14*, *23*). (**B**) E vs. Fm relationships for all soils (green circles, orange triangles) and LiWu POC (white diamonds) in which RPO fraction ^{14}C activity was measured. Marker sizes represent the relative amount of total OC contained in each RPO fraction. Constraints on end-member E and Fm ranges are described in the main text (blue, vascular-plant OC$_{bio}$; gray, OC$_{petro}$). Black arrows represent theoretical trends for end-member mixing (vertical) and chemical alteration (horizontal) (*23*) and indicate that alteration is necessary in order to explain the presence of mid-E OC. For both panels, dashed lines separate OC into low-E (<150 kJ mol^{-1}), mid-E ($150 \leq E <$ 185 kJ mol^{-1}), and high-E ($\geq$185 kJ mol^{-1}) regions. Fm error bars are smaller than marker sizes.

417

418
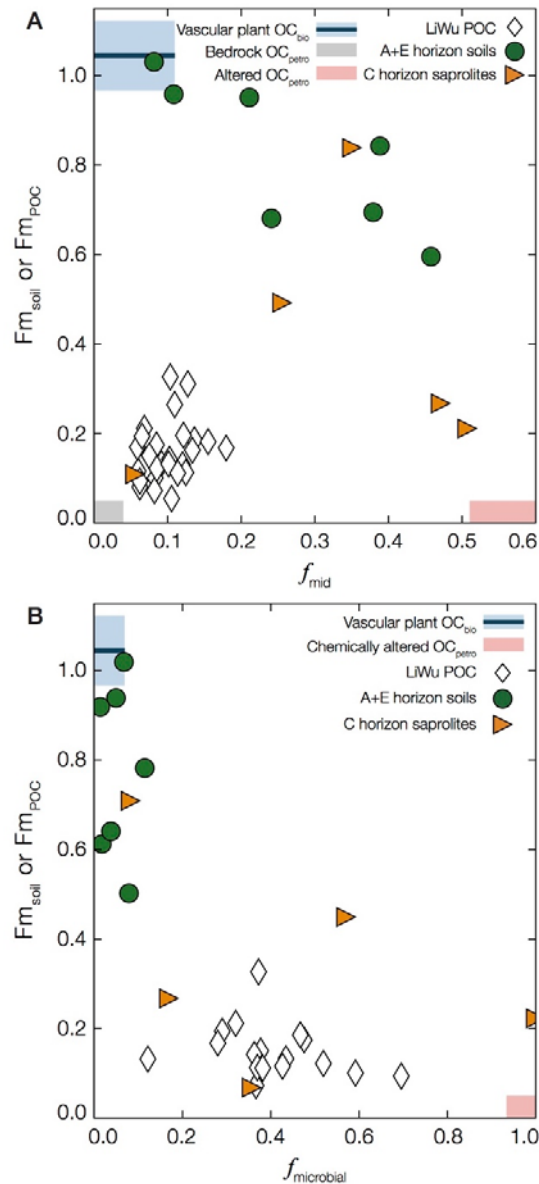
Fig. 3. Evidence for microbially mediated bedrock OC oxidation. (**A**) Bulk Fm vs. f_{mid}
relationships for soil (green circles, orange triangles) and LiWu POC (white diamonds). All soils,
with the exception of the 0.5 m saprolite discussed in the main text, are described by a mixing
line between vascular-plant OC_{bio} (blue) and chemically altered OC_{petro} (red) (*14*). LiWu River
POC is dominated by bedrock OC (gray) but does contain detectable chemically altered OC_{petro},
as evidenced by the deviation from a vertical mixing line between OC_{bio} and OC_{petro}. (**B**) Bulk
Fm vs. $f_{microbial}$ relationships for all samples in which fatty acid concentrations were analyzed
(*14*). The relative abundance of microbial fatty acids increases with decreasing Fm across all
samples, suggesting that microbial respiration is the source of chemically altered OC_{petro}.
Measurement error bars are smaller than marker sizes.

14

429